Size segregation, convection, and arching effect

Alejandro Saez, Francisco Vivanco, and Francisco Melo*
Departamento de Física Universidad de Santiago de Chile and Center for Advanced Interdisciplinary Research in Materials, Avenue Ecuador 3493, Casilla 307 Correo 2 Santiago, Chile
(Received 14 February 2005; published 31 August 2005)

We present a numerical study based on the contact dynamic procedure for the size segregation in a two-dimensional vibrating container. In agreement with previous studies, we find that the rising of the larger particle is accompanied by convection rolls. However, at low enough acceleration, rolls do not penetrate the entire cell and a local vault mechanism is observed, in which the larger particle moves up by steps. This mechanism, described in experiments by Duran and co-workers [Phys. Rev. E. **50**, 5138 (1994)], occurs in a very narrow region of parameter space. Once the larger intruder reaches the exponential tail of convecting roll, its vertical motion becomes continuous and the corresponding rising speed is dramatically increased.

DOI: 10.1103/PhysRevE.72.021307 PACS number(s): 45.70.Mg, 64.75.+g, 83.80.Fg

Up to now, among the variety of phenomena exhibited by granular material, size segregation remains one of the most puzzling [1,2]. In a granular mixture of equal density beads, in contrast to ordinary fluid or gases where particles are distributed according to their density, larger particles are found to rise to the top of the mixture. This effect, of importance in numerous industrial processes, has been studied extensively both experimentally [3–5] and numerically. For instance, Rosato *et al.* [6] proposed a Monte Carlo algorithm in conjunction with a kinetic argument to explain segregation as a consequence of the larger mobility of smaller particles. Jullien *et al.*, [7] using a piling technique to mimic the segregation process, obtained a critical ratio $\eta_{\min} \sim 3$ of the radius of the large to the small particles below which no segregation occurs. From the experimental point of view, it has been clearly shown that segregation and convection are strongly connected [8,9]. In most of the experiments, the larger particles are carried up by the ascent flux due to the convecting rolls. However, Duran and co-workers [10] presented experimental evidence for two types of dynamics. In a two-dimensional arrangement, in addition to the convective regime, they observed the discontinuous ascent of the larger particle. Motivated by these findings and numerical predictions [7], these authors [11] formulated a geometrical theory involving local arching, in which the intruder may not have homogeneous contact with the underlying small particles and is rather supported by two lateral walls lying at an angle of 60° with respect to the horizontal, which corresponds to the angle of repose of the two-dimensional (2D) monodisperse piling. In this picture, the small particles glide down along the surface of the rising intruder, which moves by discrete jumps of amplitude of the order of one particle diameter. In addition, a new critical ratio $\eta_{CD} \sim 13$ is found by these authors, which separates the discontinuous from the continuous rising. For $\eta > \eta_{CD}$ rising of intruder takes place continuously.

Further numerical simulations developed by Jullien *et al.* [12] have shown some evidence of the discontinuous dynamics by including horizontal random fluctuations into a heuristic model. More recently, Pöschel *et al.* [13] developed a molecular dynamics method to show that the rising of the larger particle is always accompanied by convection cells, even in the case of lowest possible frequency. Although no discontinuous rising up is observed by these authors, they suggested that the mechanism of local arching might control how the larger particle moves into the exponentially weak convection before being lifted upwards. To our knowledge, numerical simulations based on first principles have not yet captured the main features of the local arching effect.

In this article, we present numerical simulations based on the contact dynamics method in which, in addition to the segregation due to convection, we reproduce the discontinuous rising of the intruder and recover features similar to those observed experimentally by Duran *et al.* [10]. In agreement with Pöschel's idea [13], we have found that the mechanism of segregation by discrete jumps appears close to the exponential tail of the convecting rolls. It is important to notice that the mechanism of convection we address here is produced by walls friction and not by air flow through the porous granulate. In addition, our simulations are carried out at the low-frequency regime where convection is always present. At high frequency, as reported in Ref. [1], when convection is suppressed, fluidization of the granular bed may cause either buoyancy or sinking of the intruder, depending on density. In the presence of air, it has been shown [14] that even the so-called "reverse buoyancy" for which light intruders move to the bottom, might take place.

A detailed description of the contact dynamics method developed by Moreau and Jean can be found in Ref. [15]. Basically, this method is a time integration of the dynamical equations, at level of the velocities, of a system of colliding particles, which does not consider any force of repulsion to regularize the non-smooth contacts. The method consists in finding a set of after-collision velocities and contact reactions from the knowledge of before-collision velocities that satisfy the contact laws referred to the impenetrability of particles and the mutual friction. The impenetrability of hard particles is treated using the velocity Signorini condition. This condition establishes that if the normal component of the separation velocity of two particles is positive, then the normal mutual force exerted is zero. On the other hand, if the par-

*Electronic address: fmelo@lauca.usach.cl

ticles are in contact or equivalently, the separation velocity is zero. Then the normal force takes a sufficiently positive large value to prevent particle interpenetration. In addition, the friction is taken into account through Coulomb's friction law, which establishes that if the sliding velocity is nonzero, then the friction force resists the sliding and takes a value proportional to the normal force μN. On the contrary, if the sliding velocity is zero, then the friction force remains in the interval $[-\mu N, \mu N]$. The proportionality constant μ is known as the friction coefficient. The dynamics of each particle in the system is described by the equations of linear and angular momentum conservation. Thus, the equations for the particle i, in contact with a set of particles labeled by k, read,

$$m_i(\vec{v}_i^{+} - \vec{v}_i^{-}) = \sum_k (\vec{R}_{ik}^{n} + \vec{R}_{ik}^{t}), \tag{1}$$

$$I_i(\vec{\omega}_i^{+} - \vec{\omega}_i^{-}) = \sum_k \vec{r}_i \times \vec{R}_{ik}^{t}, \tag{2}$$

where m_i is the ith-particle mass, I_i its moment of inertia and r_i its radius. The linear and angular velocities are represented by $\vec{v}_i$ and $\vec{\omega}_i$, respectively. The minus signs indicate before collision state and the plus signs after collision states. Finally, $\vec{R}_{ik}^{n}$ and $\vec{R}_{ik}^{t}$ are the impulses generated by the impact forces (reactions) during the collisions in the normal and tangential directions, respectively. A similar set of equations can be written for the particle j in contact with the particles labeled by l. In order to handle elastic collisions, Moreau and Jean introduced a generalized relative velocity constructed as a weighted average of before and after collision relative velocities

$$\vec{u}_i = \frac{1}{1+\rho_i}\vec{v}_i^{+} + \frac{\rho_i}{1+\rho_i}\vec{v}_i^{-}, \tag{3}$$

where ρ_i is the restitution coefficient (for a detailed discussion on these generalized velocities, see Ref. [15] and references therein). For binary collisions this coefficient coincides with the Newton's restitution coefficient. Usually, these equations are separated in normal and tangential projections and the corresponding restitution coefficients must be included. Finally, from the set of projected equations, the values for after-collision velocities and reactions for the active contacts can be obtained using an iterative process.

Here, to approach the experimental conditions developed in Duran's work [10], we consider 3300 particles of diameter $d=1.5$ mm, contained in a box with 50 particles width and 66 layers in depth. We initially take an intruder size $D=13d$ ($\eta=13$), since near this particular value it is expected to observe a transition from discontinuous to continuous intruder rising [10]. We have considered for the restitution and friction coefficients $\rho_n=0.6$, $\rho_t=0.6$, and $\mu=0.97$, respectively, for all particles including the intruder. These values correspond approximatively to those of aluminum particles used in experiments [16]. The restitution and friction coefficients of the bottom of the container are taken equal to those of the particles. In most the calculations presented here, the lateral walls have equal elastic and friction properties than the particles. However, some results obtained for frictionless laterals walls and for periodic boundary conditions are discussed in the conclusion section as well. Our container oscillates vertically following a sinusoidal displacement at frequency f and amplitude A. Thus, the main control parameters are f and the dimensionless acceleration $\Gamma=A(2\pi f)^2/g$, where g is the gravity acceleration. The frequency of oscillation is taken constant at 15 Hz, as in the experiment [10], whereas the amplitude of oscillation varies from 1.1 to 2.2 times the particle's diameter. Thus, Γ varies from 1.5 to 3.0.

To characterize the convection intensity we use a convection flux Φ as defined by Pöschel [13]. Φ is the sum of material mass flow in the center of the box j_{top} and the flow close to the walls j_{bot}. Since j_{top} and j_{bot} are defined positive here, Φ is different from zero in the convective regime. For a given horizontal position of the cell, the flows j_{bot} and j_{top} are calculated by adding the number of particles that move to the bottom and to the top, respectively, and is expressed in number of particles per cycle time. In practice, as in Ref. [13], we measure for each particle if the positions at the subsequent nodes of the vibration are on different sides of a horizontal line. The height of the cell was divided into 100 horizontal lines between the container bottom and the free surface of the granular compact. The initial configuration of the particles is a disordered packing and is obtained as follows. The intruder is initially located centered at the bottom of the container and the small particles are distributed in a random loose packing around it. Then, in the absence of vibration, the system is left to reach a compacted configuration by the action of gravity for about a minute of system real time. With this rule, some vacancies close to the intruder and some small domains of hexagonal packing are observed. Then the vibration is turned on and the time evolution of the system is followed for 15 min. The time step was set to 1 ms since we checked that our numerical calculations produce similar results for shorter time step.

In the upper panel of Fig. 1 we present the vertical position of the intruder as a function of time, for several accelerations Γ. To obtain these data we record the intruder position at every cycle, when the box is at maximum upward speed. For low enough values of Γ, see curves 1, 2, and 3 of this panel, three regimes can be identified as time evolves. At early stages, a fast rise of the intruder is observed whereas at intermediate stages, the intruder motion is very slow or may even cease for a while. At later stages, always the intruder accelerates quickly until it reaches the top layer. In contrast, at higher values of Γ (curves 5, 6, 7, and 8) the intermediate regime disappears and the intruder moves quickly to the free surface. Let us describe in more detail the curve 1 included in the upper panel of Fig. 1. The early fast motion of the intruder occurs when most of the particles located close to the lateral walls move downward, pushing the intruder upward. Notice that such a rapid upward motion at the beginning of the ascent has been reported in experiments, see Fig. 3 of Ref. [10]. We observe here that this motion is just due to the fact that the system tries to produce convection rolls of the size of the entire cell, see Fig. 2(b). However, after a short time of about 20 s, the downward motion of the particles located at the lower portion of the walls cell ceases and the convection rolls continue to develop gradually from the

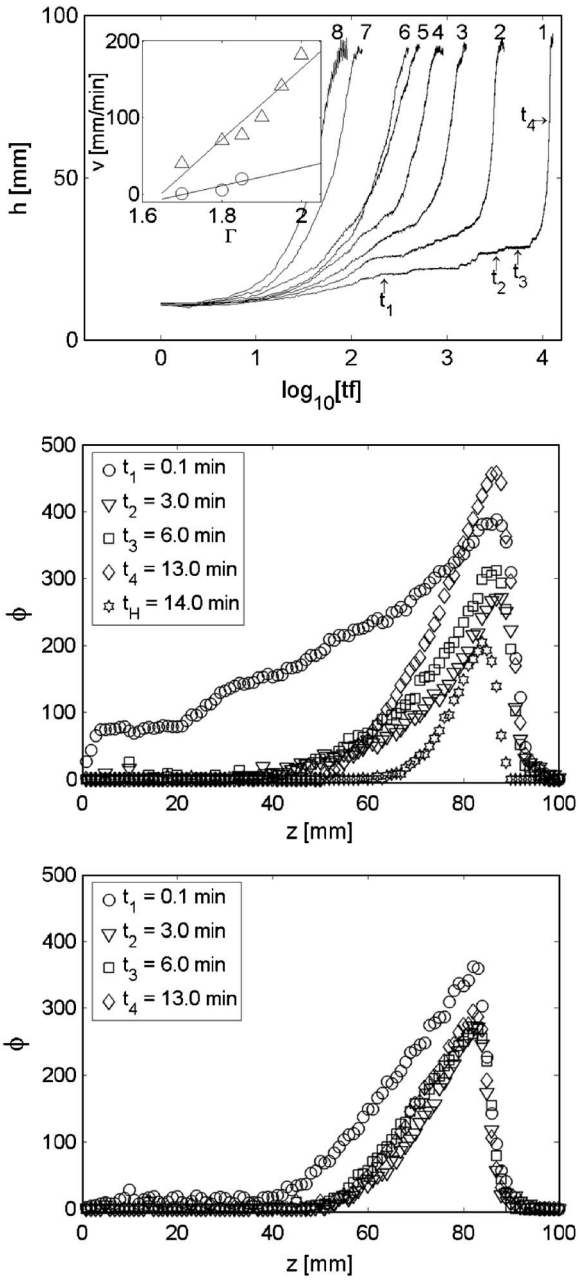

FIG. 1. Upper panel: The vertical position of the intruder, measured at the subsequent nodes of the oscillating box, as a function of $\log_{10}(ft)$, for a constant frequency $f=15$ Hz, and different values of acceleration. $1:\Gamma=1.75$, $2:\Gamma=1.8$, $3:\Gamma=1.85$, $4:\Gamma=1.9$, and $5:\Gamma=1.95$, $6:\Gamma=2.0$, $7:\Gamma=2.5$, and $8:\Gamma=3.0$. Inset, intruder time-average speed as a function of Γ, for the vault and convective regime, circles and triangles, respectively. Middle panel: the convection intensity Φ, in the presence of the intruder, as a function of depth at several time stages t_1-t_4, t_H corresponding to the time when the intruder reaches the free surface. Lower panel: convection intensity Φ in the absence of the intruder at the same time stages t_1-t_4.

top of the layer. This behavior is quantitatively illustrated in the middle panel of Fig. 1, where for the same value of Γ corresponding to the curve 1 of the upper panel, we present the convection intensity Φ as a function of depth at several

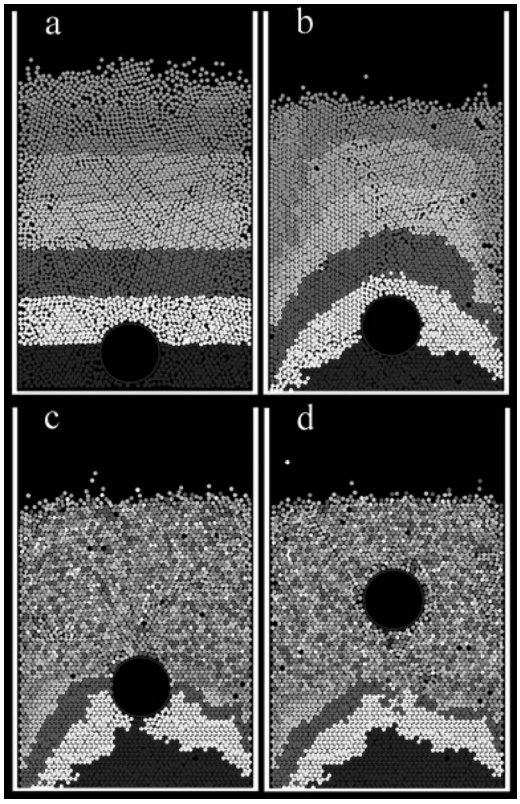

FIG. 2. Snapshots of the convecting particles and intruder segregation at different times t. For $f=15$ Hz and $\Gamma=1.7$. (a) At early stages $t=0.01$ min, all the particles located close to the vertical walls move downward, producing a fast motion of the intruder. Gray-scale sections, initially flat, curve themselves upward due to this motion. (b) $t=0.2$ min, the initial convection ceases at the lower regions of the cell (this occurs for low value of Γ). Thus, further deformations of the gray sections at these regions are no longer observed and convecting rolls develop progressively from the surface of the layer. (c) $t=9$ min, when the intruder center has reached the exponential tail of convection, it is lifted up by the ascent current. (d) $t=13$ min, fast rise of the intruder when trapped by the ascent convecting current. This configuration can be compared to Fig. 2(c) in Ref. [10].

times. At early stages, Φ does not vanish as we move down into the cell, whereas at later stages, Φ shows a clear exponential decrease and therefore a well defined vertical penetration distance of the rolls. Notice that roll penetration increases slowly as time progresses.

At first glance, the intruder's vertical motion seems to cease on the nearly flat region of the curve 1 (upper panel of Fig. 1). However, a detailed observation indicates that the intruder moves slowly upward by vertical jumps. These jumps, of size of the order of a particle diameter, correspond to the small steps displayed by the curve 1 and 2 (upper panel of Fig. 1). The vertical speed of the intruder in this regime, as depicted on the inset of the upper panel of Fig. 1, is about 1 mm/min at low Γ but increases rapidly, indicating that the number of jumps become more frequent with Γ. It is important to realize that when discontinuous jumps occur, the vertical penetration of convection rolls is still small but the convecting tail probably influences regions located right

above the intruder. As time progresses, the intruder moves slowly into the convecting tail, whereas the convecting rolls develop slightly deeper, as seen in the middle panel of Fig. 1. The fast rise begins when the intruder center reach the exponential tail of convection. Notice that this situation which is illustrated in Fig. 2(c), is quite similar to the one reported in Fig.2(b) of Ref. [10]. In the convective regime, see Fig. 2(d), the characteristic velocity of the intruder is of the same order as the velocity of the particles moving up. On the other hand, the intruder's presence effect on the convection can be obtained by comparing the middle and the lower panel of Fig. 1. At early stages of the process, the penetration of convection rolls is dramatically increased by the presence of the intruder. By contrast, once the intruder reaches the free surface of the compact, indicated by t_H on the middle panel of Fig. 1, convection intensity becomes smaller than that in the absence of an intruder. We note that previous results depend on the initial packing of the bed, a point which will be discussed later in the text.

At high Γ, in agreement with previous numerical works [13], a discontinuous motion is never observed; the intruder is quickly trapped by the upward part of the rolls and moves continuously to the top. This regime was described by Pöschel [13] and therefore it is not presented here in detail. However, our data allow us to extract further information on intruder speed V, as a function of Γ, for given intruder size and frequency. The inset of the upper panel of Fig. 1 depicts the time average speed in the convective regime, indicating that V is a strong increasing function of Γ.

In the following, we study the discontinuous motion of the intruder observed at low Γ and its connection with the arching mechanism invoked in Ref. [11]. First, it is important to check that such a motion is not related to the global convective current but instead to the local gliding of small particles located right below the intruder. For this purpose, we have tracked with a time resolution of 1 ms, the angular position θ of the nearest-neighbor particles of the intruder. To define the nearest neighbors, we considered all the particles inside a window of $1.5d$ radial size, measured from the intruder border. Therefore not all neighbors are in close contact with the intruder. For each nearest neighbor, θ is followed in a time interval, 6 s long and centered at t_1, which includes one of the intruder vertical jump visible in curve 1 on Fig. 1. As time progresses, it is seen in Fig. 3, that the particles' trajectories are curved toward $\theta=0$, indicating that gliding of particles has occurred. This gliding which appears as the spatio-temporal defects on Fig. 3 is not continuous and occurs by steps of the angular position of some of the nearest particles around the intruder. The rise time of these angular steps ranges from half to roughly five oscillation periods (i.e., 0.066 s to 0.33 s for $\Gamma=1.75$), its average being about 1.5 cycles. When monitoring the exact phase of the oscillating box, at which nearest neighbor start gliding, a rather flat distribution is observed, i.e., there is no a preferential part of the cycle for which this motion is triggered. Some vacancies are observed near the intruder's bottom, see, for instance, Fig. 2(b). Since near these vacancies the particles have larger mobility, discontinuous vertical rising of the intruder is observed whenever a small particle glides down along the surface of the larger particle. Additional numerical calculations with smaller intruders show similar features.

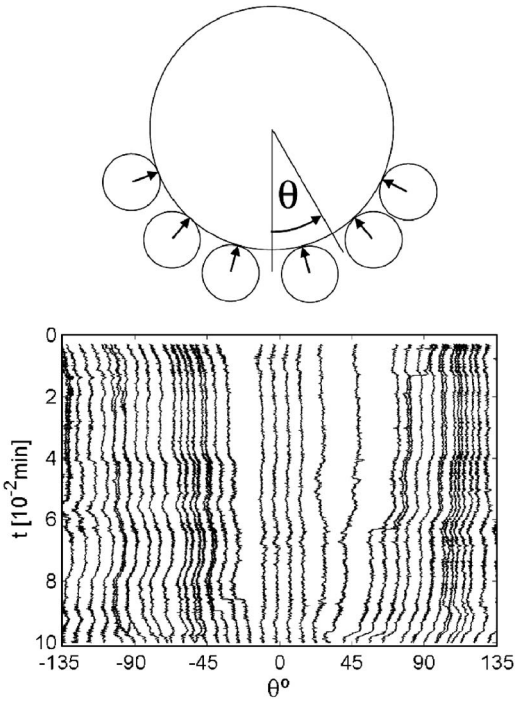

FIG. 3. Upper panel: Schema of the nearest particles located around the intruder, labeled by the coordinate θ. Lower panel: Time evolution of the angular positions of the particles located close to the intruder, with time resolution of 1 ms, for the vertical intruder step observed in curve 1 of Fig. 1, around t_1. For $\Gamma=1.7$ and $f=15$ Hz. Notice that as time evolves (increasing toward the bottom of the figure), a collective motion of small particles occurs toward the intruder bottom.

To characterize the interaction of the nearest neighbors with the intruder, we have calculated the normal impulsive force acting on the intruder as a function of the angular position θ, Fig. 4. This force is averaged over a time interval of 6 s and it is displayed at three different stages, labeled by t_1, t_3, and t_4, exhibited by the curve 1 of Fig. 1. In Fig. 4(a), the force is averaged in a time interval that includes the same vertical jump analyzed in Fig. 3 (i.e., centered at t_1). If the arching mechanism is taking place, it is expected to observe an impulsive force that has several maxima for the angles corresponding to the position of the particles sustaining the intruder. Consistently, since this mechanism requires the intruder be sustained mainly by lateral forces, a force minimum around $\theta=0$ is expected as well. From our numerical calculations, we observed that the force indeed has these features. Moreover, a well-defined maximum might be observed close to $\pm 60°$ consistent with a hexagonal packing. This occurs notoriously in the case of Fig. 4(a) mainly at the left side of the intruder, where the packing is high enough. In contrast, at the right-hand side of the intruder the number of vacancies is slightly higher, allowing larger mobilities of small particles and therefore, the angular spreading of the force. Similar features are observed in Fig. 4(b), which illustrates the force calculated at the time interval centered at t_3, where vertical jumps of the intruder are not present. In this case, consistent with the absence of any jump, the force is relatively spread out. In addition, we have plotted in Fig. 4(c)

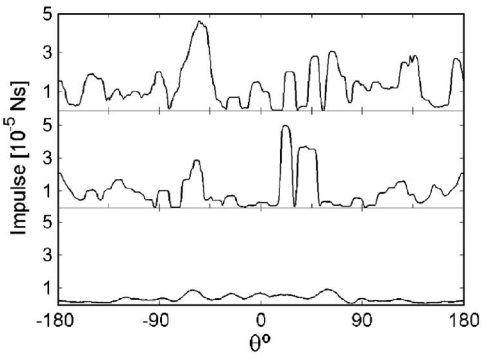

FIG. 4. Time average over 6 s of the normal impulse acting on the intruder as a function of the angular position θ, for constant frequency $f=15$ Hz and $\Gamma=1.7$. (a) Average during a time interval that includes a single jump up exhibited by curve 1 on Fig. 1, around t_1. For the arching regime, a maximum of the impulse is observed at the left side of the intruder. At the right side, due to the mobility of small particles associated to the higher concentration of vacancies, the impulse is spread out. (b) Average over a time interval, which does not exhibit any jump up of the intruder, obtained in the flat part of curve 1 on Fig. 1, around t_3. (c) Average around t_4, in the convective regime.

the average normal force (around t_4) when the intruder is carried up by the convecting rolls.

Consistent with the absence of arching, the force is dramatically spread out. Thus, we have observed the two main ingredients of the arching mechanism, namely, the existence of vacancies that allows particle gliding just below the intruder and the force localization at the packing angle characteristic of vault effect.

To complete this study, we investigate how convection intensity and penetration vary with the initial packing of the particles. In addition to the disordered packing described above, a hexagonal packing is investigated. To arrange a hexagonal packing, as in the experiments [10], the intruder is located centered at the bottom of the container and the small particles are positioned one by one around it forming a hexagonal arrangement. In the hexagonal configuration the contact forces are distributed along lines forming an angle of $\pm 60°$ with respect to the horizontal. Thus, two defect lines, about 10 particles wide oriented as the contact forces, which propagate along the entire system, are generated by the presence of the intruder. All these features are present in the experimental configuration used in Ref. [10]. By contrast, in the disordered packing the contact forces can be found in a nearly isotropic distribution and the perturbation introduced by the intruder is localized only in its neighborhood. In Fig. 5, for all parameters kept constant, we compare the convection intensity Φ for the two choices of packing in the presence of the intruder. In both cases the convective arm penetrates quickly the system whole height, as shown in Figs. 5(a) and 5(c). The main difference between both situations occurs at early stages of the development of convection. Compare for instance, data in Figs. 5(b) and 5(d) taken at $t=0.1$ min. This effect can be explained by the particles' ability to slide. Certainly, the disordered packing has more voids available than the hexagonal one, which facilitates the particle movements and consequently the development of the

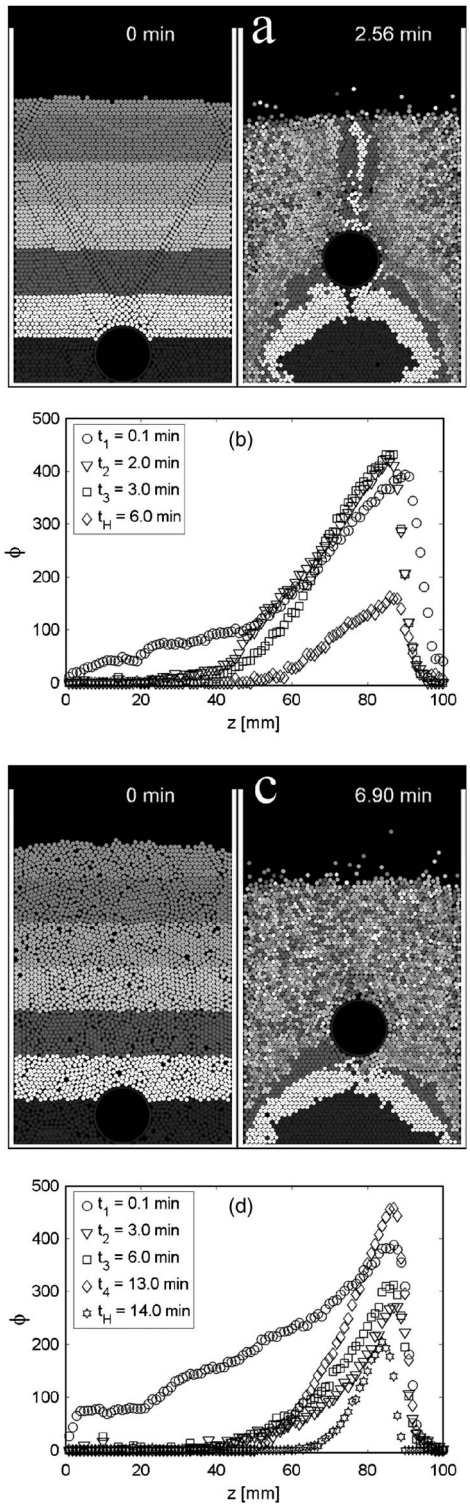

FIG. 5. Effect of packing on segregation intensity Φ. (a) Snapshots of hexagonal packing case. (b) The corresponding convection intensity Φ. (c) and (d) Similar to (a) and (b) for the disordered packing. In both cases, $\Gamma=1.7$, $\eta=13$, and $f=15$ Hz.

convection at deeper distances. Notice that, after the vertical forcing is turned on, the disordered packing evolves to hexagonal one in a time which is of the order of 20 s. At later stages, the intensity of convection is slightly larger for the hexagonal packing and as time passes this difference is

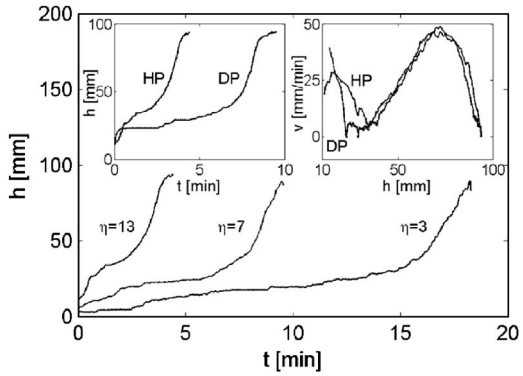

FIG. 6. The vertical position of several size intruders as function of time, for a constant frequency $f=15$ Hz and a constant acceleration $\Gamma=1.7$, for an initial hexagonal packing. Intruder to particle diameter ratio from left to right; $\eta=13$, $\eta=7$, and $\eta=3$. The left inset shows the rise times for the hexagonal packing (HP) and the disordered packing (DP), for $\eta=13$. Right inset compares the intruder speed in the convective regime for HP and DP packing

slowly increased, compare Figs. 5(b) and 5(d). In turn, the penetration distance of rolls seems to be very similar in both cases. There is another important feature of the experiment reported in Ref. [10] that is well captured here. Experimentally, as the intruder moves up into the convecting rolls, the convection intensity underneath is dramatically decreased. This is well observed in Figs. 5(b) and 5(d) when contrasting Φ, calculated when the intruder has reached the surface t_H, to earlier values of Φ.

We now discuss how the segregation velocity depends on the intruder's size and how initial packing influences the rise time. Figure 6 shows the vertical position of intruders of several sizes as a function of time, for constant frequency and vertical acceleration, for a hexagonal initial packing. As before, three different regimes of intruder vertical motion are observed. In many previous experiments and numerical calculations, roughly the ascent velocity is an increasing function of the intruder's size. In our case, by taking the average slope in Fig. 6, for the arching regime, the intruder speed increases approximatively as $V_{\mathrm{vault}}^{\mathrm{int}} \sim (0.6D/d - 1.4)[\mathrm{mm/min}]$. Experimentally, a similar linear law is reported in Ref. [10] for the vault regime but with a clear minimum size $D \sim 3d$, for which the intruder rising up is no longer observed. Although our calculations do not show strong evidence for the existence of this minimum size, this is not in contradiction with experimental results in Ref. [10]. Indeed, in experiments, such threshold value is sensitive to the vibration amplitude, the cell aspect ratio, and the position of the intruder into the cell.

When the intruder is trapped by the convecting current, the ascent speed results about four times larger than that in the vault regime, being still linear with D, $V_{\mathrm{conv}}^{\mathrm{int}} \sim (2.5D/d + 14)[\mathrm{mm/min}]$. We believe that this is a manifestation of the effect of the intruder size in the convective intensity, the larger the intruder the larger the convective intensity. Otherwise, the intruder speed would be size independent. It is interesting to examine what happens when the box is so wide that its laterals walls are much further away from the large particle than the height of the packing. Our calculations performed in a box 200 particles wide and 60 particles height, for $\Gamma=2$, when locating the intruder at the bottom and centered on the box, show that one roll develops quickly from each laterals wall. These rolls that extend over the entire depth are nearly symmetric, with a lateral extension that is close to the layer height. As time progresses, the induced friction produces the gradual development of two new rolls, of similar size at the center of the box, that progressively trap the intruder. The intruder seems to follow passively the convective current, moving up and down alternatively at a nearly constant speed. In this situation, for relatively small intruders ($\eta < 13$) and the box dimensions used here, the size of the intruder does not seem to affect dramatically the convective current. Naturally, since isolated rolls from each wall develop laterally at a distance equal to the layer height, it is reasonable to assume that the optimal width of the box for convection is twice its height. One important point that remains to be checked is whether or not this optimal width is also the critical width for which the rise speed is no longer a function of the intruder size.

The left side inset of Fig. 6 contrasts the corresponding vertical position of intruder as a function of time when disordered and hexagonal initial packing are used. It is seen that the intruder's rise time can be reduced by a factor 2 with the hexagonal packing. However, in the convecting regime the rise speed is similar for both initial packing, as seen in the right side inset of Fig. 6. Thus, this subtle rise time decrease must be due to either differences of the ascent speed during the vault regime, or some packing rearrangements taking place at the earliest development of convecting arms affecting the intruder position. The left inset of Fig. 6 shows that the early development of convecting arms, responsible for the first fast rise of the intruder, would be more effective in the disordered packing locating the intruder slightly higher in the convecting tail. However, the left inset of Fig. 6 also shows relatively more frequent activity of the vault effect for an hexagonal packing. Thus, it seems difficult to conclude which mechanism dominates the strong decrease on rise time observed for a hexagonal packing.

In conclusion, we believe that the simulations reported above capture qualitatively well the main features of the arching mechanism invoked in Ref. [10]. There are, however, some differences that do not allow us to make precise quantitative comparisons with experiments. For instance, in the present calculation the intruder was located at the container bottom, whereas in the experiments it is placed at a height of 1.5 cm from it. The effect of the initial location of the intruder was first recognized by Pöschel [13] and later observed experimentally by several authors, see, for instance, Ref. [1]. It is well known that higher initial positions of the intruder decrease the rise time in a complex way. Another difference with the experiments is that simulations exhibit convection at some larger value of acceleration, $\Gamma_{\mathrm{sim}}=1.70$ than experiments, $\Gamma_{\mathrm{exp}}=1.25$. In the experiments reported in Ref. [10], convecting rolls would have involved the entire cell for the values of Γ used in the present study. This difference is likely due to the larger values of friction coefficients used in our simulations. In our case, for relatively larger $\Gamma_{\mathrm{sim}}=1.70$, the convecting current is still localized and penetrates a fraction of the cell. This feature allows us to

observe the vault regime for Γ larger than the experimental values. Consistent with the experimental findings, see Ref. [10], when we increase Γ the convecting rolls penetrate the entire cell and the discontinuous rising is no longer observed.

An important feature of this phenomenon is qualitatively captured by our simulations. Experimentally, for Γ kept constant, a transition from discontinuous to continuous rising is observed when the intruder reaches a critical size $D_c \sim 13d$ [11]. Numerically, for the case of a disordered packing at low enough values of Γ, we do observe a remarkable discontinuous motion of a large intruder $D \sim 13d$ and a transition to a continuous rising as Γ increases. However, when a hexagonal packing is used, at low Γ, the discontinuous rising up almost disappears when the intruder size reaches $D_c \sim 13d$, see inset of Fig. 6. In addition, with this packing, the rising time calculated here and that observed experimentally are consistent. Hence, a detailed description of segregation dynamics not only depends on the initial location of the intruder but also on the packing preparation.

Finally, to our knowledge, the arching effect for segregation has never been observed experimentally in the absence of convection. In our calculations, when frictionless lateral walls were used, convection rolls and intruder rise were both suppressed. Interestingly, the same is true when walls are replaced by periodic boundary conditions. As can be deduced from Ref. [10], the main difference between the convecting and vault regimes is that in the latter the convection rolls are very weak and located above the intruder. Notice that our calculations and previous results reported in the literature [13] show that at the convection onset, the penetration of the rolls is nearly half the box width, indicating a criterium for the intruder initial location for which vault effect might be observed.

Another important difference showed by our numerical simulations is that in the vault regime the intruder influences the penetration and intensity of convection rolls. The most remarkable effect of intruder presence, consistent with experiments, is that when the intruder rises up, the convection intensity underneath is decreased notoriously. In turn, the mechanism of discrete steps by particle gliding plays an important role controlling the dynamics of the larger particle when it approaches to the zone of exponentially decreasing convection.

We are very grateful to Jean-Noel Roux for introducing us to the contact dynamics method. We acknowledge interesting comments and fruitful discussions with E. Clément and E. Hamm. This work was supported by Conicyt-Chile under Research Program Fondap Grant No. 11980002.

[1] D. A. Huerta and J. C. Ruiz-Suárez, Phys. Rev. Lett. **92**, 114301 (2004).
[2] L. Vanel, A. D. Rosato, and R. N. Dave, Phys. Rev. Lett. **78**, 1255 (1997).
[3] J. C. Williams, Powder Technol. **15**, 245 (1976).
[4] K. Ahmad and I. J. Smalley, Powder Technol. **8**, 69 (1973).
[5] J. Bridgewater, Powder Technol. **15**, 215 (1976).
[6] A. Rosato, K. J. Strandburg, F. Prinz, and R. H. Swendsen, Phys. Rev. Lett. **58**, 1038 (1987).
[7] R. Jullien, P. Meakin, and P. Pavlovitch, Phys. Rev. Lett. **69**, 640 (1992).
[8] J. Knight, H. M. Jaeger, and S. Nagel, Phys. Rev. Lett. **70**, 3728 (1993).
[9] H. M. Jaeger and S. R. Nagel, Science **255**, 1523 (1992).
[10] J. Duran, T. Mazozi, E. Clément, and J. Rajchenbach, Phys. Rev. E **50**, 5138 (1994).
[11] J. Duran, J. Rajchenbach, and E. Clément, Phys. Rev. Lett. **70**, 2431 (1993).
[12] R. Jullien, P. Meakin, and P. Pavlovitch, Phys. Rev. Lett. **70**, 2195 (1993).
[13] T. Pöschel and H. J. Herrmann, Europhys. Lett. **29**, 123 (1995).
[14] See, for instance, T. Shinbrot and F. J. Muzzio, Phys. Rev. Lett. **81**, 4365 (1998); G. Gutierrez, O. Pozo, L. I. Reyes, R. Paredes, J. F. Drake, and E. Ott, Phys. Rev. E (to be published).
[15] See, for instance J. Moreau and M. Jean, *Proceedings of the 3rd Biennial European Joint Conference on Engineering Systems Design and Analysis*, 1996, Montpellier, France, edited by J. Moreau [Eur. J. Mech. A/Solids 13, 93 (1994)]; M. Jean and J. Moreau, in *Proceedings of Contact Mechanics International Symposium*, edited by A. Curnier (Presses Romandes (1992), p. 31.
[16] E. Clément, J. Duran, and J. Rajchenbach, Phys. Rev. Lett. **69**, 1189 (1992).